Electromagnetic Emissions from DC to 17 GHz from a Pulsed Plasma Thruster (PPT)

IEPC-2007-269

Michael L. Garrett* and Edward J. Beiting†
The Aerospace Corporation, Los Angeles, CA 90009-2957 USA

Will Caven‡ and Ron Cory§
Space Systems/Loral, Palo Alto, CA 94303 USA

Measurements of electromagnetic emission from a solid Teflon® Pulsed Plasma Thruster (PPT) are reported for frequencies ranging from DC to 17 GHz. The PPT discharged 40 Joules of electric energy per pulse at a pulse rate of 0.5 Hz for all data collected in this test. Each firing of the thruster produced a double discharge that created a pair of electromagnetic pulses separated by 5 μs. Amplitude variations of as much as 25 dB between successive pulses were observed. Peak amplitudes greater than 160 dBμV/m were observed for frequency components below 50 MHz. Spatial and polarization variations in amplitude were also recorded but these variations were small relative to the shot-to-shot pulse amplitude variations. Shielding of the PPT reduced radiated electric emissions approximately 20 dB from 10 kHz to 17 GHz.

Nomenclature

AF	=	Antenna Factor
dB	=	Decibel
dBpT	=	Decibels referenced to 1 picoTelsa
dBμV/m	=	Decibels referenced 1 microVolt/meter
DSO	=	Digital Sampling Oscilloscope
DRH	=	Double Ridge Horn antenna
EMC	=	Electromagnetic Compatibility
EMI	=	Electromagnetic Interference
FFT	=	Fast Fourier Transform
Log-P	=	Log periodic antenna
LNA	=	Low Noise Amplifier
MIL-STD-461	=	Military EMC Standard
PPT	=	Pulsed plasma thruster
P-rod	=	Passive rod antenna
RBW	=	Resolution Band Width
RE	=	Radiated Emission
V-Pol	=	Vertical Polarization
H-Pol	=	Horizontal Polarization

* Associate Technical Staff, Propulsion Sciences, M2-341, michael.l.garrett@aero.org
† Senior Scientist, Propulsion Sciences, M2-341, edward.j.beiting@aero.org
‡ Spacecraft Payload Systems Engineer, caven.will@ssd.loral.com
§ Spacecraft Propulsion Subsystems Engineer, cory.ron@ssd.loral.com

I. Introduction

The Pulsed Plasma Thruster (PPT) became the first electric propulsion device flown in space when the Soviet Union launched the Zond 2 spacecraft in 1964.[1] During the subsequent four decades of development, research, and testing, it has been established that the PPT emits significant electromagnetic energy. This emission has been documented for frequencies ranging from DC to 18 GHz and has the potential to lower the sensitivity of onboard communication receivers.[2-6] Although the emission is short duration (<1 ms) and infrequent (PPT firing generally occurs at approximately 1 Hz), it is important to characterize the structure and amplitude of this electromagnetic emission for integration onto a spacecraft bus.

A solid Teflon® PPT, manufactured by Aerojet, was tested at The Aerospace Corporation from 14 June to 3 October 2005 under a contract with Space Systems/Loral, the purpose of which was to determine compatibility of PPTs with various spacecraft payloads. This PPT is a 40 J-class, rectangular geometry thruster. Emissions from this thruster in the 1nm to 13,500nm spectral region are reported in another paper at this conference.[7] The objectives of this work were to characterize the PPT with respect to spacecraft contamination potential, electromagnetic compatibility, and plume emission at wavelengths from the soft x-ray to the mid-infrared. Space Systems/Loral provided the Modular Test Unit PPT[8], a set of drive electronics, and the wiring harness. Aerospace provided the vacuum chamber, anechoic room, test instrumentation, and facility data systems. This paper describes the electromagnetic compatibility (EMC) studies and is organized into five sections. The results are summarized for the electric field emissions in Section III. The AC magnetic field emissions are discussed in Sections IV. Conclusions are presented in Section V.

II. Facility, Configurations, and Test Sequence Guidelines

The measurements were taken in the Aerospace Electric Propulsion Facility.[9] The PPT is located in a 0.9 m diameter, 1.5 m long fiberglass tank attached to the side of the main chamber for all EMC testing (see Fig. 1).

EMC Facility

The Aerospace Corporation EMC facility comprises three components. The first is a small, all-dielectric vacuum tank that houses the thruster or other test article. This fiberglass tank is largely transparent to electromagnetic radiation and mates to a stainless steel vacuum chamber that is 2.4 m in diameter and 9.8 m long. The main chamber housed 7 cryopumps with a nominal throughput for xenon of 220,000 l/s and has a base pressure of 1 x 10^{-8} mbar. The second component, a semi-anechoic room, surrounds the dielectric tank to shield the thruster from the ambient electromagnetic environment. This metallic room is lined with 0.6-m-high pyramids that absorb radiation from the thruster at frequencies higher than 80 MHz to mitigate reflections from the walls of the room. The final component is a set of calibrated receivers that record the radiation emanating from the thruster. Each receiver connects sequentially to a series of antennas through a panel in the semi-anechoic room using a two-section semi-rigid cable with known attenuation. The arrangement of these components is shown in Fig. 1.

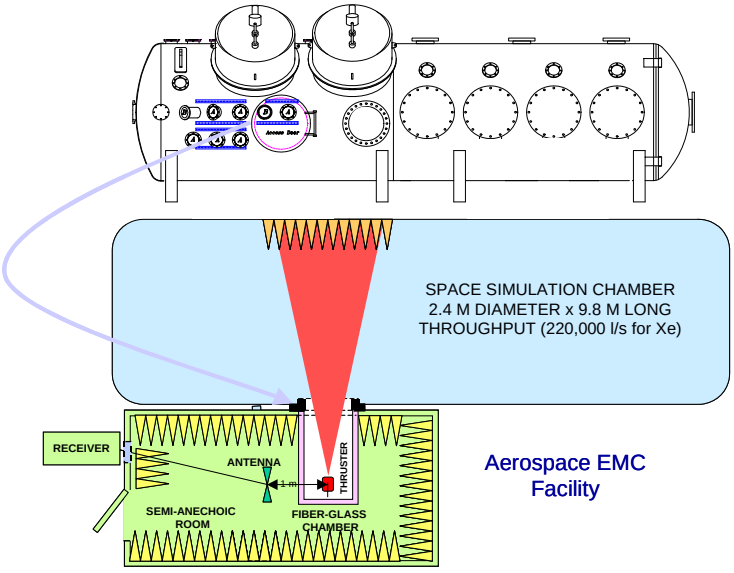

Figure 1. Layout of the facility used to measure electromagnetic emissions from PPT

A scale drawing of the anechoic room and fiberglass tank is presented in Fig. 2. The pyramid-lined 5 m x 3 m x 3 m semi-anechoic room surrounding the tank provides >100 dB shielding from 14 kHz-18 GHz (MIL-STD-285 and NSA 65-5 compliant). The interior of the room is covered with AEP-24 absorber with the exception of a 2-m-high by 1-m-wide section covered with AEP-8 absorber adjacent to the dielectric tank. All bolts, fittings, water lines,

flanges, and support fixtures within and attached to the fiberglass tank are fabricated of electrically non-conducting materials with the exception of the L-bracket supporting the thruster.

The small size of the fiberglass tank allows antennas to be placed outside the vacuum to the side and behind the thruster at a distance of one meter from the thruster as required by MIL-STD-461E. Because the antennas are outside the vacuum, there are no concerns of antenna-plasma interaction. Additionally, the antennas required for recording emission between 10 kHz and 18 GHz (or higher frequencies) can be positioned sequentially, eliminating the possibility of antenna-antenna interaction.

The plume of the thruster exhausts into the main vacuum tank and terminates on a beam dump comprising an array of 0.6-m-high aluminum pyramids that are covered with flexible graphite to reduce sputtering by the high-energy ions. The pyramidal design of this conducting beam dump serves to reduce scattering of electromagnetic radiation from the thruster by the main tank at frequencies greater than 80 MHz.

At frequencies above 1 GHz, interference effects and absorption from the wall of the fiberglass become non-negligible. The transmission coefficient of an S2 fiberglass wall of 1 cm thickness undergoes sinusoidal oscillations with a period of 7.5 GHz. The calculated and measured transmission through the fiberglass wall indicates that periodically the radiation measured outside the chamber is too low by 2.3 to 3.0 dB. Additional information on the EMC facility is available.[9,10]

Figure 2 shows a top view of the anechoic room, including the relative positions of the dielectric tank and the main vacuum chamber. Positions 60H through 285H mark the antenna positions used during the campaign. For each position label, the number indicates the angle, in degrees, of the antenna from the centerline of the thruster taken counterclockwise and the letter indicates the measurement plane. All positions in Fig. 2 lie in the horizontal plane bisecting the thruster on a circle of 1 m radius from the center of the PPT exhaust nozzle. Positions 90C and 180C represent the magnetic field loop locations, which were positioned 52 cm and 50 cm from the PPT, respectively.

Figure 3 illustrates the vertical test configuration. A wooden support structure was fabricated to position the antennas in a vertical plane coinciding with the exit plane of the PPT. For each position, the number represents the angle, in degrees, of the antenna from the centerline of the thruster taken clockwise from the bottom.

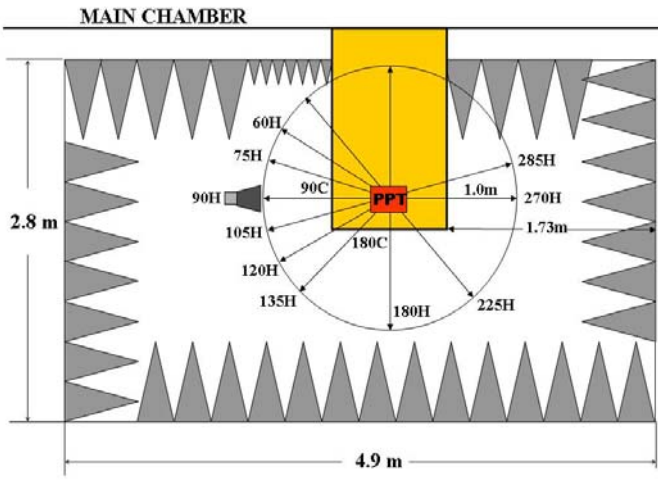

Figure 2. Scale drawing of anechoic room showing antenna and thruster placement

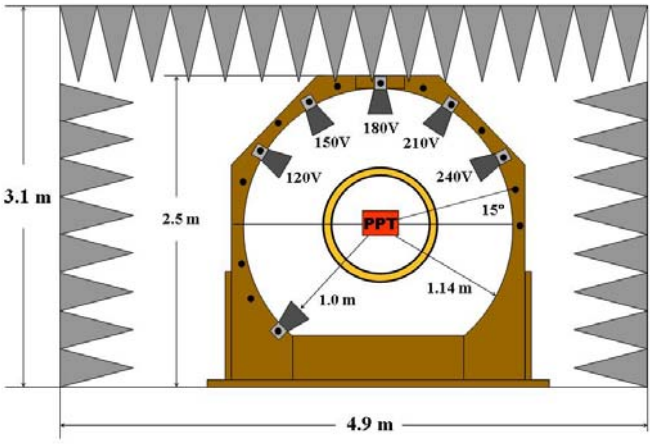

Figure 3. Vertical test configuration showing antenna and thruster positions.

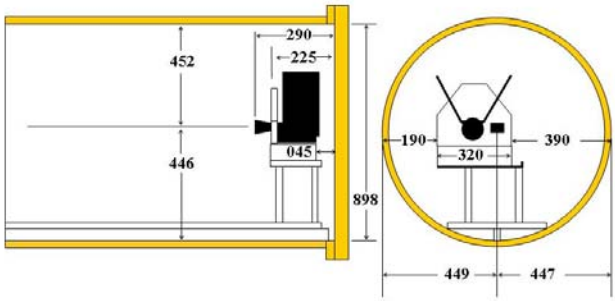

Figure 4. Diagram of PPT in dielectric tank. All dimensions in mm.

The mounting geometry with dimensions of the PPT in the dielectric tank is shown in Fig. 4. Here the thruster was placed in the dielectric tank and exhausted its plume orthogonally to the axis of the main vacuum chamber. The thruster was attached to an aluminum plate such that the back of the PPT was 45 mm from the inside of the back flange of the tank. The base plate was 200 mm wide and 350 mm long and was supported by four 2.54 cm diameter fiberglass rods. The PPT was mounted such that its centerline nearly coincided (within 3 mm) with the axis of the fiberglass tank but was offset from the axis horizontally by 100 mm. This effectively positioned the PPT nozzle along the axis of the chamber. The distance from the fiberglass back flange to the exit plane of the thruster was 290 mm. Electrical leads were routed along the bottom of the dielectric chamber underneath a fiberglass plate. Note that the PPT was oriented for all tests such that the spark pug and cathode were closest to position 270H whereas the anode was closest to position 90H in Fig. 2. By this convention, the cathode is on the left and the anode is on the right in Fig. 5c, below.

III. Radiated Electric Field Emissions

Both temporal and spectral radiated electric field measurements were made on the PPT. Radiated electric fields were recorded at multiple positions around the PPT at a distance 1 meter from the thruster. The time domain studies will be discussed first, followed by a discussion of the spectral measurements.

Figure 5. PPT in dielectric tank: a) unshielded configuration; b) shielded configuration; c) PPT front side viewed from main vacuum chamber

Time Domain RE Measurements

For each measurement, data were taken at a repetition rate of 0.5 Hz for 200-second durations to accumulate 100 pulses to allow for statistical analysis. Four antennas were used to span the 10 kHz to 17 GHz frequency range measured: An EMCO 3303 Passive Rod for 10 kHz to 30 MHz; An EMCO 3109P Biconical for 30 MHz to 200 MHz; An EMCO 3148 Log Periodic for 200 MHz to 1GHz; and an EMCO 3115 Double Ridge Horn for 1 GHz to 18 GHz. A Tektronix TDS 6154C 15 GHz Digital Sampling Oscilloscope (DSO) was used for all time domain measurements. Each antenna was connected through a Storm 5.5 m coaxial cable, a bulkhead feed-through, and a Storm 2.4 m coaxial cable to the oscilloscope terminated in 50 Ohms. Measurements were made in the unshielded configuration (shown in Fig. 5a) for all positions illustrated in Fig. 2 and Fig. 3. After data were taken in Bands 1 through 4, the PPT was shielded (Fig. 5b) and data were collected at position 90H for each of the four bands. A synopsis of all time domain data is presented in Table 1. Each measurement band is shown with its frequency range, transducer, transducer polarization and all positions in both vertical and horizontal planes where data were acquired.

The PPT firing comprises two main events, separated by the charging of the PPT's capacitors. First, the spark plug ignites and ablates a small number of particles that provide a path between the electrodes. Once this conducting path has formed, the main capacitor discharges across the electrode gap, ablating a layer of Teflon® particles. Figure 6 illustrates a typical pulse from the PPT. The data in Fig. 6 were acquired using a passive rod antenna with a bandwidth extending from 5 MHz to 50 MHz. In Fig. 6a, the first pulse corresponds to the spark igniter, which is followed approximately 5μs later by the main discharge initiation. Figure 6b reveals the transformed frequency spectrum. The raw transform data are given in units of mV for reference, and then converted to corrected electric field units of dBμV/m. The peak at approximately 23 MHz is the primary contribution of the

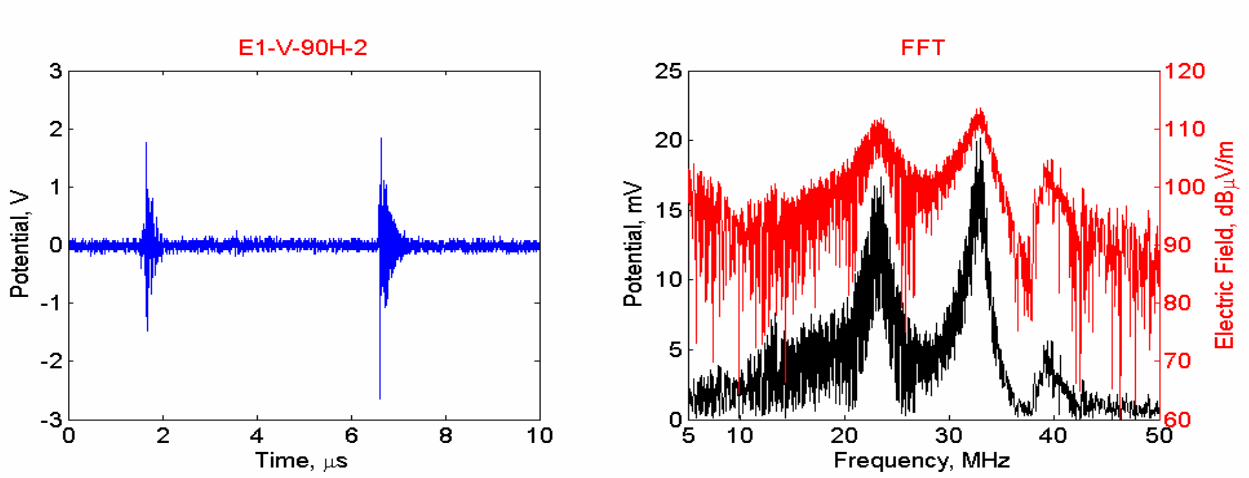

Figure 6. Typical PPT pulse: a) shows the observed time domain pulse, while b) shows the transformed frequency spectrum. The upper data correspond to the right vertical axis, while the lower data correspond to the left vertical axis.

spark igniter whereas the peak at 33 MHz is the dominant frequency component from the main discharge initiation pulse. It is important to recognize that Fig. 6 represents a single pulse from the PPT. Due to the large shot-to-shot variation of pulses, most of the analysis presented in this paper represents statistical data that were accumulated from 100 distinct pulses.

Table 1. Synopsis of Temporal Measurements

Measurement	Frequency	Antenna	Polarization	Positions
Band 1	10 kHz - 50 MHz	Passive Rod	V	90H
Band 2	30 MHz - 200 MHz	Biconical	V&H	90H
Band 3	200 MHz - 2 GHz	Log Periodic	V&H	90H, 180H, 270H, 180V
Band 4	1 GHz - 15 GHz	DRH	V&H	60H - 280H, 120V - 240V
Band 1 Shield	10 kHz - 50 MHz	Passive Rod	V	90H
Band 2 Shield	30 MHz – 200 MHz	Biconical	V&H	90H
Band 3 Shield	200 MHz – 2 GHz	Log Periodic	V&H	90H
Band 4 Shield	1 GHz – 15 GHz	DRH	V&H	90H, 180H
AC Magnetic	DC – 1 MHz	ETS 7604	V&H	90C, 180C

For each of these 100 pulses, the DSO executed an FFT to compute the corresponding frequency spectrum, which was saved with the temporal data. Following data collection, the time-domain pulses were also transformed with a standard FFT algorithm, viz.,

$$X(k) = \sum_{j=1}^{N} x(j)\exp[-2\pi i(k-1)(j-1)/N] \qquad 1 \le k \le N \tag{1}$$

The results of this transform correlated well with the internal Tektronix FFT algorithm once converted into electric field units of dBμV/m. The standard algorithm executes most efficiently for data sets that are a power of two in length. Therefore the next highest power of two beyond the data length was chosen and the data were padded with zeros. The magnitude of the FFT was obtained by taking the absolute value of the FFT divided by the length of the data. The electric field amplitude was obtained from the FFT magnitude by the following relationship:

$$E = 20\log[10^6 \cdot |E_0|] + AF \tag{2}$$

where E is in units of dBμV/m, E_0 is electric pulse FFT magnitude in units of volts, and AF is dB/m. The corresponding frequency mapping of the FFT amplitude was accomplished by taking the reciprocal of the time resolution divided by the length of data. The effective Resolution Band Width (RBW) of the FFT was calculated using:

$$RBW\ (3dB) = 0.88 \cdot \frac{1}{\Delta T \cdot N} \tag{3}$$

where ΔT is the time resolution of the pulse trace and N is the number of samples. The coefficient 0.88 is the number of FFT bins corresponding to a 3 dB RBW for a rectangular window.[11] Table 2 provides the FFT bins and effective RBWs for each measurement band. Each measurement band is shown with its transducer, frequency range, timebase resolution, number of sample points, FFT bin size and effective resolution bandwidth.

Table 2. Table of RE FFT Bins and Effective RBWs

Band #	Antenna	Frequency Range	ΔT	N	FFT Bin Size	RBW(3dB)
1a	P-Rod 1	10kHz - 5MHz	2ns	5k	100kHz	88kHz
1b	P-Rod 2	5MHz - 50MHz	2ns	5k	100kHz	88kHz
2	Bicon	30MHz - 200MHz	800ps	12.5k	100kHz	88kHz
3	Log-P	200MHz - 2GHz	200ps	50k	100kHz	88kHz
4	DRH	1GHz - 15GHz	25ps	32k	1.25MHz	1.1MHz
1M	ETS 7604	20Hz – 1MHz	8ns	5k	25kHz	22kHz

For the 5 MHz to 50 MHz band (Passive Rod, Band 1b), it was possible to characterize the maximum electric field of the pulse directly from the time domain pulse. This was achievable because most of the radiated energy falls within this band manifested in two peaks observed near 20 MHz and 30 MHz and because the antenna factor is relatively constant across this band. In Fig. 7, the maximum amplitude, in volts, from the time domain pulse was converted directly into electric field values using the antenna factor at the maximum pulse height within the FFT spectrum. Both unshielded and shielded configurations are plotted. The unshielded configuration produced pulses with an average magnitude of 152 dBμV/m in this band whereas the shielding added to the PPT reduced the pulse magnitude by 21 dB to 131dBμV/m.

In addition, analysis was done on pulse amplitude scaling as a function of measurement bandwidth. Hoskins[3] suggests that the EO-1 PPT produces an average coherent pulse approximately 1 MHz in width. This is consistent with our observation that the average pulse from the PPT is approximately 1μs in duration. Therefore, when scaling bandwidth below 1 MHz, it is reasonable to assume that the pulse is primarily coherent. Because coherent radiation increases 20 dB in magnitude for each decade increase in bandwidth, pulses are scaled 20 dB per decade change in bandwidth for bandwidths narrower than approximately 1 MHz. Likewise, when scaling above 1 MHz, it is reasonable to use an incoherent assumption about the radiation and scale pulses at 10 dB per decade change in bandwidth. Using these criteria, the maximum pulse amplitude was scaled from the 88 kHz effective RBW used to compute the FFT, to the 45 MHz bandwidth of the passive rod antenna. As shown in Table 3, there is a reasonable correlation between the absolute amplitudes (shown in Fig. 7 and Table 3a) and scaled values from the FFT (shown in Table 3b).

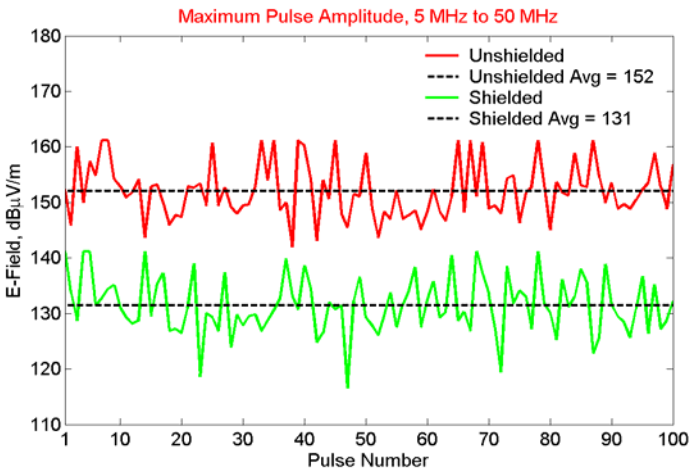

Figure 7. Maximum pulse amplitude from time domain pulse, in shielded and unshielded configurations

Table 3a shows the maximum electric field directly calculated from the time domain pulse. Because the spectrum contains two discrete maximum peaks (see Fig. 6), which occur at frequencies where the antenna factor is relatively constant, the absolute electric field can be estimated within the bandwidth of the antenna. The maximum amplitude observed on the DSO ("TD pulse maximum", in Table 3.) is converted to an electric field magnitude using Eq. (2). Table 3b shows the maximum electric field computed by scaling the windowed FFT electric field from the original bandwidth to the actual effective bandwidth available to the DSO. Again, the pulse amplitude is scaled using a coherent radiation assumption from 88 kHz to 1 MHz and an incoherent radiation assumption from 1 MHz to the 45 MHz bandwidth of the passive rod antenna.

Table 3. Table of RE FFT Bins and effective RBWs

Table 3 a

Band	TD pulse maximum	Peak F	AF	Ant BW	Calculated E-Field
P-rod-2-Unshielded	5 V	30 MHz	27 dB/m	45 MHz	161 dBuV/m
P-rod-2-Shielded	0.5 V	20 MHz	26 dB/m	45 MHz	140 dBuV/m

Table 3 b

Band	FFT pulse maximum	Bin Size	Window	RBW (3dB)	Scaled E-Field*
P-rod-2-Unshielded	124 dBuV/m	100 kHz	Rectangular	88 kHz	162 dBuV/m
P-rod-2-Shielded	103 dBuV/m	100 kHz	Rectangular	88 kHz	141 dBuV/m

*FFT pulse maximum scaled at 20dB/decade from 88 kHz to 1MHz, and 10dB/decade from 1 MHz to 45MHz

Figures 8 and 9 illustrate signal levels across the entire spectrum measured for vertically and horizontally polarized emissions. The data represents the maximum electric field amplitudes observed at position 90H for the resolution bandwidths indicated. For each frequency band, 100 time domain pulses were transformed via Eq. (1), into frequency spectra. The maximum amplitude for each frequency point within these spectra was then plotted in Figs. 8 and 9. It is important to emphasize that the data in a given spectrum are a composite of emission from 400 (V-Pol) or 300 (H-Pol) distinct pulses. The effective RBWs and measured emissions are shown in Fig. 8. In Fig. 9 the data are scaled to Mil-STD 461E RBWs. This bandwidth scaling is plotted for factors of both 20 dB and 10 dB per decade increase in RBW as discussed above. The actual emission lies between the upper (10 dB) and lower (20 dB) lines at a level, which depends on exactly how coherent each pulse is at a given frequency. Note that above 30 MHz the MIL-STD RBW varies only slightly from the original RBW in which the data were taken. For this reason, the data scaled at 20 dB and 10 dB per decade are comparable.

Conclusions about the relative amplitudes among these pulses are not highly quantitative; Fig. 7 shows that pulse-to-pulse variations of 15 dB are not uncommon. The "PPT OFF" data in Figs. 8 and 9 represent the instrument sensitivity. These data are scaled 10 dB per decade change in bandwidth in Fig. 9 because they represent the incoherent noise of the measurement system. Note that the emission is not above the sensitivity of the instrumentation for portions of the spectrum. The sensitivity of the shield data is better than that of the unshielded data because a higher gain could be used on the oscilloscope due to the lower signal levels encountered.

The response of the facility for the positions in Figs. 2 and 3 was calculated and used to evaluate data presented in this paper. A three-step procedure was used to generate calibration terms. First, a self-contained comb generator about the size of the PPT, was placed 1 meter from the antenna in an open area of the semi-anechoic room with no obstructions between the antenna and generator. (The absorption of the pyramids' semi-anechoic room is sufficient to eliminate wall and ceiling reflections above 1 GHz.) The unobstructed antenna-generator geometry duplicated the geometry between the antenna and thruster. The comb generator (Com-Power CG-5118) produced a stable emission every 20 or 100 MHz with a frequency limit of about 15 GHz. A computer program extracted the peak of the comb emission. Second, the comb generator was placed in the dielectric chamber in the exact location where the thruster would be placed and the antenna was placed at one of the positions shown in Figs 2 and 3. A frequency scan that was identical to the unobstructed scan was then taken. These measurements were repeated for each of the antenna locations. Third, the obstructed measurements were normalized by the direct measurements for each position. This procedure created the correction terms that are added to the data. Measurements were taken for both antenna polarizations.

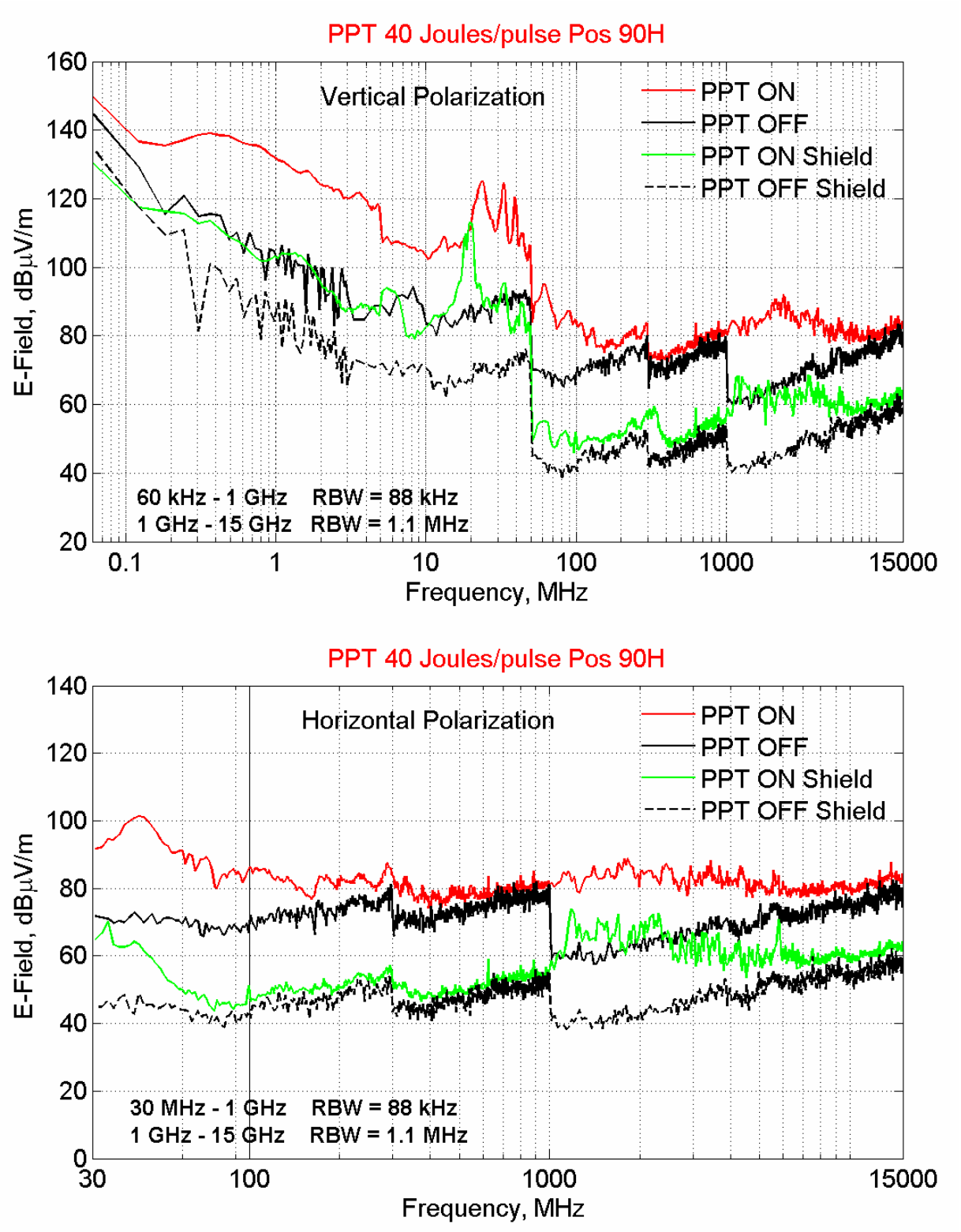

Figure 8. Measured PPT spectral emissions and RBWs, position 90H a) Vertical polarization, b) Horizontal polarization

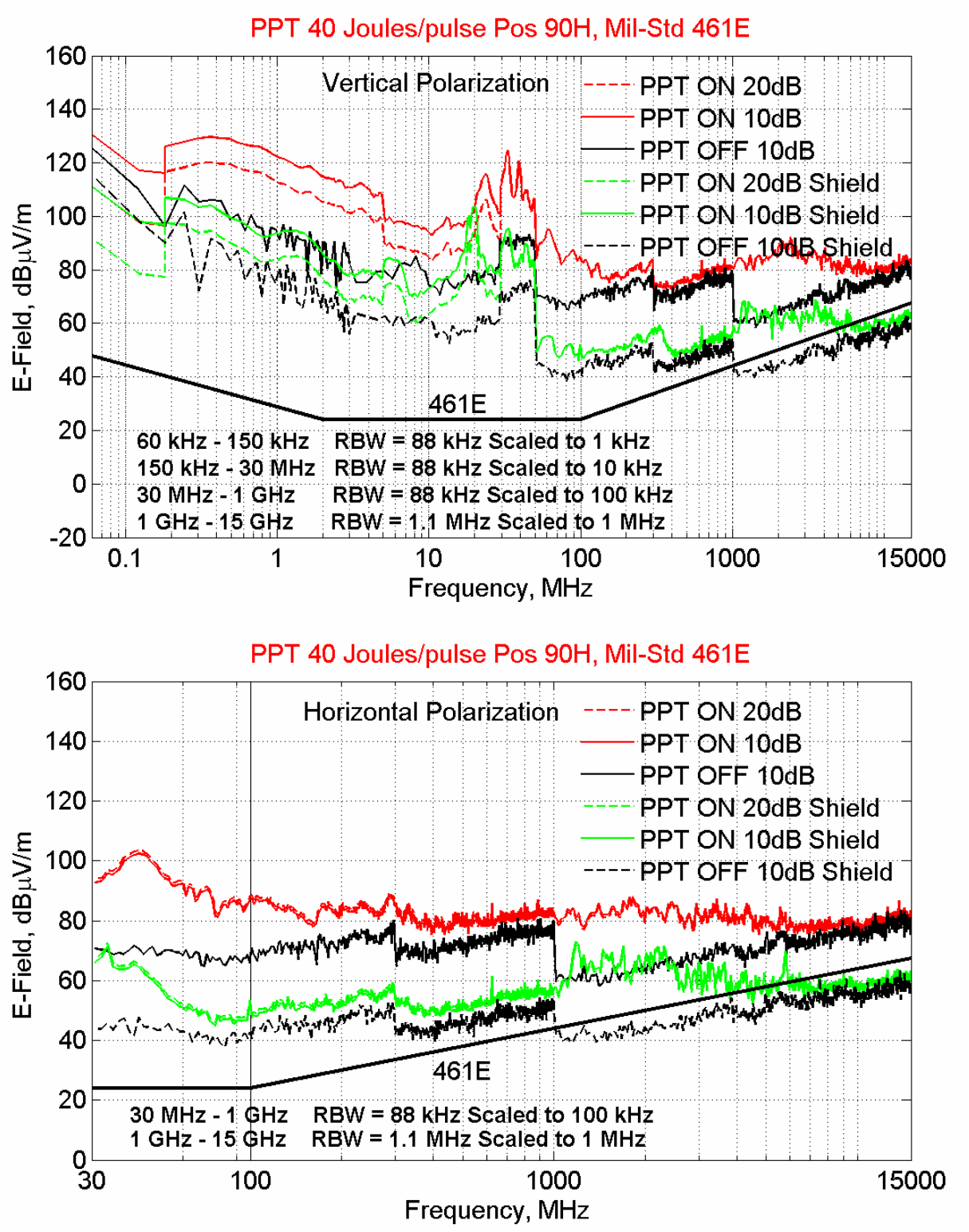

Figure 9. PPT spectral emissions scaled to Mil-STD 461E RBWs, position 90H a) Vertical polarization b) Horizontal polarization

Spectral Zero Span Measurements

The PPT was operated at 0.5 Hz for all measurements. Data was taken for 200-second durations to accumulate 100 pulses for statistical analysis for each measurement. Measurements were taken at four discrete frequencies: 401 MHz, 1275 MHz, 1375 MHz, and 1730 MHz with the analyzer in zero span mode. Figure 10 shows data which were taken at 1275 MHz, at position 90H, for both shielded and unshielded PPT configurations.

Table 4. Synopsis of Spectral Measurements

Measurement	Frequency	Antenna	Polarization	Position
Band 1	401 MHz	Log P	V&H	60H, 90H, 120H, 180H, 225H, 270H, 180V
Band 2	1275 MHz	DRH	V&H	60H, 90H, 120H, 180H, 225H, 270H, 180V
Band 3	1375 MHz	DRH	V&H	60H, 90H, 120H, 180H, 225H, 270H, 180V
Band 4	1730 MHz	DRH	V&H	60H, 90H, 120H, 180H, 225H, 270H, 180V
Band 1 Shield	401 MHz	Log P	V&H	90H
Band 2 Shield	1275 MHz	DRH	V&H	90H
Band 3 Shield	1375 MHz	DRH	V&H	90H
Band 4 Shield	1730 MHz	DRH	V&H	90H

Measurements were made for both shielded and unshielded configurations at positions listed in Table 4 using an Agilent 8565EC spectrum analyzer with a 1 MHz RBW. For these measurements, the antenna was connected to the spectrum analyzer via two Storm coaxial cables (5.5 m and 2.4 m) using a bulkhead connector. Data was taken at 1275 MHz, 1375 MHz, and 1730 MHz using an EMCO 3115 DRH, connected to a Miteq 1-18 GHz LNA. For the 401 MHz data an EMCO 3148 Log Periodic antenna was used without a LNA. Representative data are shown in Fig. 10 with and w/o shielding for 1275 MHz. Data taken at 1375 MHz and 1730 MHz are similar in amplitude and pulse-to-pulse variation. Emission at 401 MHz however, was up to 20 dBμV/m greater than the other three frequencies. The emissions measured at 1275 MHz, 1375 MHz, and 1730 MHz were highest at positions 60H and 180H. However, emissions measured at 401 MHz were highest at position 90H. At 1275 MHz and 1375 MHz, vertically polarized emissions were higher than horizontally polarized emissions. At 401 MHz, horizontally polarized emissions were higher than vertically polarized emissions. At 1730 MHz there is no appreciable difference between the two polarizations. Shielding reduced emissions approximately 20 dB from 10 kHz to 15 GHz.

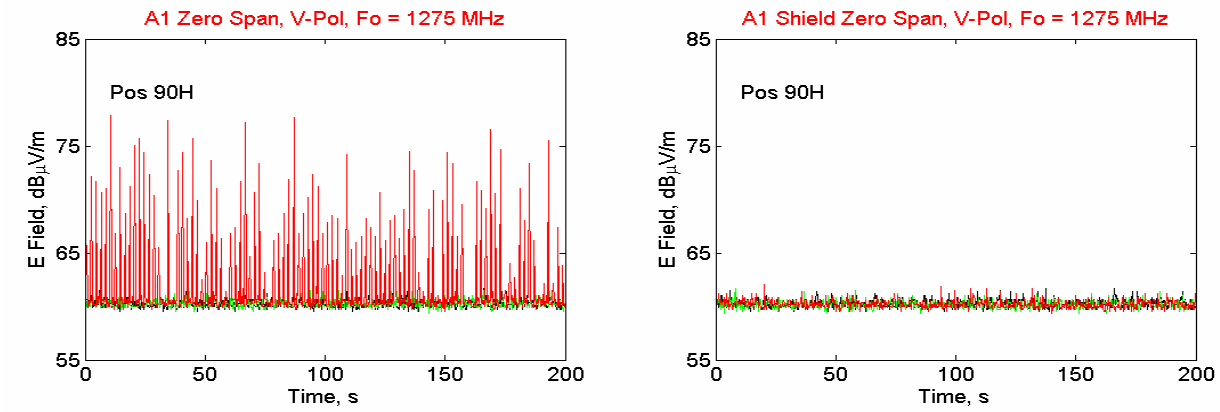

Figure 10. One hundred zero span pulses taken at postion 90H, at 1275 MHz a) Unshielded PPT, b) Shielded PPT

IV. Radiated AC Magnetic Field Measurements

Radiated AC Magnetic fields were measured at the side and back of the PPT for three orthogonal transducer orientations: X, Y, and Z. An ETS 7604 magnetic field pickup coil was used for all measurements. The distance from the coil to the PPT was 52 cm on the side of the PPT at position 90C and 50 cm from the rear of the PPT at

position 180C, as shown in Fig. 2. Measurements were made over the entire 1-MHz transducer bandwidth. These measurements were made in the time domain with a Tektronix 6154C DSO. One hundred pulses were taken while the PPT operated at 0.5 Hz at each position and orientation. Each spectrum represents a 40 μs acquisition. The time domain data was converted to frequency space using the same FFT algorithm, Eq. (1), used for the RE data. The potential for each pulse was converted to magnetic field, using:

$$B = 20\log[10^6 \cdot |B_0|] + TF \tag{4}$$

where B is in units of dBpT, B_0 is the magnetic pulse FFT magnitude in units of volts, and the Transducer factor, TF is in dBmV/pT. The primary AC magnetic component of the pulse had a frequency of approximately 100 kHz. This corresponds to the main discharge oscillation of approximately 100 kHz[1]. The Z orientation measured a pulse amplitude 10 to 15 dB higher than either the X or Y orientations. Position 90C (side) showed amplitudes as high as 130 dBpT in the Z orientation, 112 dBpT in the X orientation, and 118 dBpT in the Y orientation. Magnetic field amplitudes measured at position 180C (rear) reached 135 dBpT in the Z orientation, and 120 dBpT in the X and Y orientations. Position 180C measured 5 to 10 dB higher than position 90C. The Y orientation measured higher than the X orientation at the position 90C by a factor of approximately two. The X and Y orientations measured similar amplitudes at the positions 180C and 90C. All magnetic field values are calculated using an effective RBW of 22 kHz (refer to Table 2). The amplitudes observed represent negligible interference with magnetic field instrumentation used in some spacecraft payloads.

V. Conclusions

This report presents temporal, spectral and zero span time domain data on the electromagnetic emission from an Aerojet EO-1 Pulsed Plasma Thruster. Radiated electric emissions were studied from DC to 17 GHz and magnetic emissions were studied below 1 MHz. Pulses occurred in pairs separated by approximately 5 μs. The initial pulse from each pair corresponds to the spark igniter whereas the second pulse represents the main discharge from the PPT.

The highest-amplitude frequency components of the pulses were below 50 MHz and there was a shot-to-shot variation of up to 25 dB between successive pulses. Peaks greater than 160 dBμV/m at 100 kHz, 23 MHz, and 33 MHz were observed. For band 4 (1 – 18 GHz), horizontally polarized emissions were higher than vertically polarized emissions at positions 75, 120 and 180. However, vertical polarization produced the largest pulse amplitudes at positions 225 and 270. The measured emissions at positions 60, 90, 105, 135 and 285 were similar (within 1 dB) for both polarizations. Above 1 GHz Positions 60 and 120 produced the highest mean emissions, whereas positions 105 and 180 produced the lowest mean emissions. The remaining positions: 75, 90, 135, 225, 270, and 280 revealed similar mean emissions (within 2 dB). The spatial and polarization variation among mean pulse amplitudes within band 4 was found to be within 15 dB for all positions and polarizations. Evidently, the shot-to-shot variation among individual pulses is significantly higher than variation due to spatial orientation.

Shielding reduced electric field emission by approximately 20 dB from 10 kHz to 15 GHz. For the zero span data, the shielding reduced emission below the sensitivity of the spectrum analyzer for measurements at 1275 MHz, 1375 MHz and 1730 MHz. The 401 MHz data show a shielding effectiveness of approximately 25 dB. The data taken in at 1275 MHz, 1375 MHz, and 1730 MHz show a minimum shielding effectiveness of 17, 13, and 11 dB respectively. However, the shielded temporal data reveals approximately 20 dB of pulse attenuation across all bands. The magnitude of emissions observed to fall within typical spacecraft communications payload frequency ranges could be accommodated through a combination of shielding and coordination of link usage and thruster operation.

Acknowledgments

James E. Pollard operated of the vacuum facility and PPT during these measurements. Nicole Meckel of Aerojet provided engineering support for the PPT throughout this work. This research was made possible under a contract with Space Systems/Loral. This work was partially supported by The Aerospace Corporation's Independent Research and Development Program. All trademarks, service marks, and trade names are the property of their respective owners.

References

[1]Burton, R. L., Turchi, P. J., "Pulsed plasma Thruster," *Journal of Propulsion and Power*, Vol. 14, No. 5, Oct. 1998, pp. 716-735.

[2]Hoskins, W. A., Rayburn, C., Sarmiento, C., "Pulsed Plasma Thruster Electromagnetic Compatibility: History, Theory, and the Flight Validation on EO-1," AIAA-2003-5016, 39th *AIAA/ASME/SAE/ASEE Joint Propulsion Conference & Exhibit*, Huntsville, Alabama, 20-23 July 2003.

[3]Zakrzwski, C., Davis, M., Sarmiento, C., "Addressing EO-1 Spacecraft Pulsed Plasma Thruster EMI Concerns," AIAA-2001-3641, 37th *AIAA/ASME/SAE/ASEE Joint Propulsion Conference & Exhibit*, Salt Lake City, Utah, 8-11 July 2001.

[4]Sovey, J. S., Carney, L. M., and Knowles, S. C., "Electromagnetic Emissions Experiences Using Electric Propulsion Systems," *Journal of Propulsion and Power*, Vol. 5, No. 5, Oct. 1989, pp. 534-547.

[5]Hirata, M., Murakami, H., "Electromagnetic Noise Measurement Study of Pulsed Plasma Thruster," AIAA-81-0722, *15th International Electric Propulsion Conference*, Las Vegas, NV, 1981.

[6]Burton, R. L., Turchi, P. J., "Pulsed plasma Thruster," *Journal of Propulsion and Power*, Vol. 14, No. 5, Oct. 1998, pp. 716-735.

[7]Beiting, E.J. Qian, J., Pollard, J.E., Russell, R.W., Caven, W., Cory, R., "Absolute Optical Emission from the Mid-infrared to Extreme Ultraviolet from the Aerojet Pulsed Plasma Thruster (PPT)," International Electric Propulsion Conference, IEPC 2007-268, Florence, Italy, 2007

[8]Hoskins, W. A., Wilson, M. J., Meckel, N. J., Campbell, M., Chung, S., "PPT development efforts at Primex Aerospace Corporation," AIAA-99-2291, *35th AIAA/ASME/SAE/ASEE Joint Propulsion Conference & Exhibit*, Los Angeles, California, 20-24 June 1999.

[9]Beiting, E. J., "Design and Performance of a Facility to Measure Electromagnetic Emissions from Electric Satellite Thrusters", AIAA-2001-3344, 37th *AIAA/ASME/SAE/ASEE Joint Propulsion Conference & Exhibit*, Salt Lake City, Utah, 8-11 July 2001.

[10]Beiting, E. J., Garrett, M. L., "Facility for High-fidelity Electromagnetic Compatibility Studies of Electric Thrusters", AIAA-2007-5329, 43rd *AIAA/ASME/SAE/ASEE Joint Propulsion Conference & Exhibit*, Cincinatti, Ohio, 9-11 July 2007.

[11]Harris, F. J., "On the Use of Windows for Harmonic Analysis with the Discrete Fourier Transform," *Proceedings of the IEEE*, Vol. 66, No. 1, January 1978, pp. 51-83.